A strain energy-based equivalent layer method for the prediction of critical collapse pressure of flexible risers

Li, Xiao; Jiang, Xiaoli; Hopman, Hans

DOI
10.1016/j.oceaneng.2018.06.042

Publication date
2018

Document Version
Final published version

Published in
Ocean Engineering

Ocean Engineering 164 (2018) 248–255

Contents lists available at ScienceDirect

Ocean Engineering

journal homepage: www.elsevier.com/locate/oceaneng

A strain energy-based equivalent layer method for the prediction of critical collapse pressure of flexible risers

Xiao Li*, Xiaoli Jiang, Hans Hopman

Department of Maritime and Transport Technology, Delft University of Technology, The Netherlands

ARTICLE INFO

Keywords:
Flexible riser
Carcass
Critical pressure
Equivalent layer method
Strain energy

ABSTRACT

Flexible risers are being required to be installed in a water depth of over 3000 m for fewer remaining easy-to-access oil fields nowadays. Their innermost carcass layers are designed for external pressure resistance since the hydrostatic pressure at such a water depth may cause the collapse failure of flexible risers. Determining a critical collapse pressure for the carcass is of great importance to the whole structural safety of flexible risers. However, the complexity of the carcass profile always makes FE analysis computational intensive. To overcome that problem, the treatment of the interlocked carcass as an equivalent layer is adopted by researchers to accelerate the anti-collapse analyses. This paper presents an equivalent layer method to enable that treatment, which obtains the equivalent properties for the layer through strain energy and membrane stiffness equivalences. The strain energy of the carcass was obtained through FE models and then used in a derived equation set to calculate the geometric and material properties for the equivalent layer. After all the equivalent properties have been determined, the FE model of the equivalent layer was developed to predict the critical pressure of the carcass. The result of prediction was compared with that of the full 3D carcass model as well as the equivalent models that built based on other existing equivalent methods, which showed that the proposed equivalent layer method performs better on predicting the critical pressure of the carcass.

1. Introduction

The ongoing ultra-deep water (UDW) exploitation requires riser systems that are able to be used beyond 3000 m water depth (Luppi et al., 2014; Vidigal da Silva and Damiens, 2016). As one key technology in subsea production systems, unbonded flexible riser has been a good choice for such exploitation due to its flexibility and corrosion resistance (Edmans, 2014; NOV, 2015; Technip, 2014). This pipelike structure comprises multiple layers with different structural and operational functions. A typical internal configuration of a flexible riser is shown in Fig. 1. The innermost carcass layer is designed for external pressure resistance while the pressure armour layer is for internal pressure resistance. These two metallic layers are separated by an impermeable polymeric inner liner and nested inside one or more pairs of tensile armours. Those layers along with other functional polymeric layers are encased in an external plastic sheath, being isolated from the external environment (Cooke and Kenny, 2014).

As operators contemplate the subsea development to a water depth beyond 3000 m, the flexible riser products are required to have adequate anti-collapse capacity to withstand a very high external pressure (Wolodko and DeGeer, 2006). The more flexible the pipe is, the less its collapse resistance becomes. The critical pressure (maximum external pressure before collapse) of flexible risers does not only depend on the pipe material properties but also on pipe geometrical properties (Suleiman, 2002). Experimental tests could be an reliable approach to determine the critical pressure but such kind of the hydrostatic tests usually costly. As for numerical analyses performed on full 3D FE models, they are quite computational intensive because of the complex interlocking cross-section and the inner contacts of the carcass. Alternatively, the treatment of the carcass as a homogenous layer with equivalent thickness is adopted by researchers to simplified the anti-collapse analysis of flexible risers. This equivalent layer model could not only boost the computational efficiency in numerical analyses but also allow the development of analytical models based on ring buckling theory (Timoshenko and Gere, 1963).

Up to now, several equivalent layer methods have been proposed to calculate the thickness for that equivalent homogeneous layer. Those methods are proposed based by imposing equity between the carcass and the equivalent layer for some properties, such as cross-sectional area, bending stiffness per length or area (Zhang et al., 2003; De Sousa et al., 2001; Martins et al., 2003; Gay Neto et al., 2009; Loureiro and Pasqualino, 2012; Tang et al., 2016). Area equivalent method is carried

* Corresponding author.
E-mail address: X.Li-9@tudelft.nl (X. Li).

https://doi.org/10.1016/j.oceaneng.2018.06.042
Received 9 March 2018; Received in revised form 8 June 2018; Accepted 13 June 2018
Available online 27 June 2018
0029-8018/

Fig. 1. Typical design of a flexible riser (NOV, 2014).

out based on the equivalence of cross-sectional areas (Zhang et al., 2003). As the cross-sectional area is the only parameter considered in this method, the actual material distribution in the carcass profile is not accounted and hence the accuracy of the prediction may not be guaranteed (Cuamatzi-Melendez et al., 2017). Considering that collapse of ring-like structures is a bending-dominated problem, two methods based on the equivalence of structural bending stiffness were presented. One equivalent method obtained the thickness through sectional bending stiffness equivalence (De Sousa et al., 2001) while the other built the equivalence through bending stiffness per length (Martins et al., 2003). However, those bending stiffness equivalent methods are unable to consider the self-contact issue of the carcass, leading to an overestimation of the actual structural bending stiffness. Recently, a method based on strain energy equivalence is proposed (Tang et al., 2016). The strain energy of the carcass was obtained through the finite element model. In this carcass model, the Dirichlet-type boundary condition was applied to ensure that only hoop strain was generated along the circumferential direction. Such a strong boundary conditions enhanced the structural stiffness of the carcass, lowering its absorbed strain energy. As a result, the thickness of the equivalent layer was underestimated.

In general, most equivalent layer methods fail to capture the actual structural stiffness of the carcass due to the neglect of contact issues of the carcass. Moreover, since those methods are only focused on determining the equivalent layer thickness, other potential equivalent properties might be missing. To solve above-mentioned problems, an equivalent method is proposed in this paper that trying to construct a layer with equivalent geometric and material properties. Those properties were determined through both strain energy and membrane stiffness equivalences. The reason of adopting the strain energy equivalence is because that no available approach can be used to calculate the actual bending stiffness of the carcass. As the strain energy absorption is directly influenced by the structural stiffness, it was chosen as a representative parameter to reflect the actual bending stiffness of the carcass. Numerical models were constructed to obtain that strain energy of the carcass in this paper. After the equivalent properties of the layer were determined, the equivalent model was built and then used to predict the critical pressure of the carcass. The prediction result was compared with that of the full 3D carcass model to verify the reliability of the proposed method. This paper is organized as follows: following the introduction, Section 2 presents the establishment of the strain energy based equivalent method. Section 3 provides a feasible FE simulation for offering strain energy to the proposed equivalent method, which were verified by the test data given in the work of Tang et al. (2016). In Section 4, the equivalent models are constructed based on the proposed method and examined by related case study. The final Section 5 concludes the work.

2. Equivalent layer method based on strain energy equivalence

When the treatment of the carcass as a homogeneous layer is adopted, the equivalent properties of the layer should be determined in order to perform a similar collapse behaviour. Many researchers impose equity between those two tubular structures for their bending stiffness since the bending stiffness is a dominant factor of the critical pressure of pipe (Timoshenko and Gere, 1963)

$$p_{e,cr} = \frac{3EI}{R^3} \tag{1}$$

where $p_{e,cr}$ is the elastic critical pressure, EI is the bending stiffness of the pipe cross-section, R is the mean radius of the pipe. The bending stiffness of the equivalent layer is determined as follow (Fergestad et al., 2017)

$$EI_{eq} = Kn\frac{EI_{2'}}{L_p} \tag{2}$$

where n is the number of tendons in the carcass layer, L_p is the pitch and $I_{2'}$ is the smallest inertia moment, K is a factor that depends on the laying angle of the carcass tendons and the moment of inertia in the section.However, the actual bending stiffness of the carcass is influenced by its inner-contact and therefore much smaller than the calculated result according to its geometric configuration. In order to solve this problem, the absorbed strain energy of the carcass is chosen to reflect its actual structural stiffness when subjecting to radial compression loads. This loading case is referred to the experimental set-up of carcass radial compression tests presented in the work of Tang et al. (2016), which is shown in Fig. 2.

The strain energy of the carcass in such a loading case needs to be extracted from corresponding numerical models, which will be elaborated in the following section. For an equivalent ring model with radial compression force P, the loading force $F=P/2$ (at the cross section A) on its one quarter model can be resolved into component forces F_r and F_θ on any cross section, as shown in Fig. 3.

Therefore, its strain energy is made up of three parts

$$\begin{aligned}
&\text{a)}\ \text{Due to axial force } F_\theta \qquad U_1 \\
&\quad = \int \frac{F_\theta^2 R(1-\nu^2)}{2AE} d\theta \\
&\text{b)}\ \text{Due to axial force } F_r \qquad U_2 \\
&\quad = \int \frac{CF_r^2 R}{2AG} d\theta \\
&\text{c)}\ \text{Due to bending moment } M \qquad U_3 \\
&\quad = \int \frac{M^2 R(1-\nu^2)}{2EI} d\theta
\end{aligned} \tag{3}$$

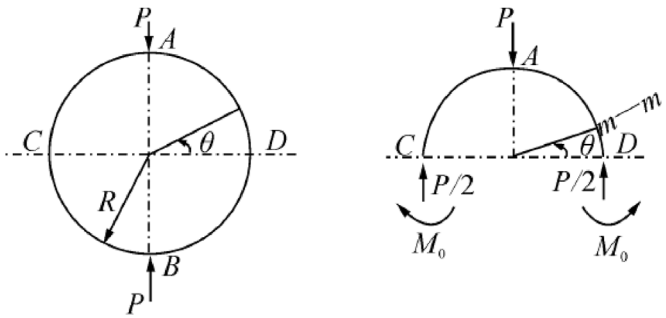

Fig. 2. Schematic diagram of a ring compressed in the radial direction (Tang et al., 2016).

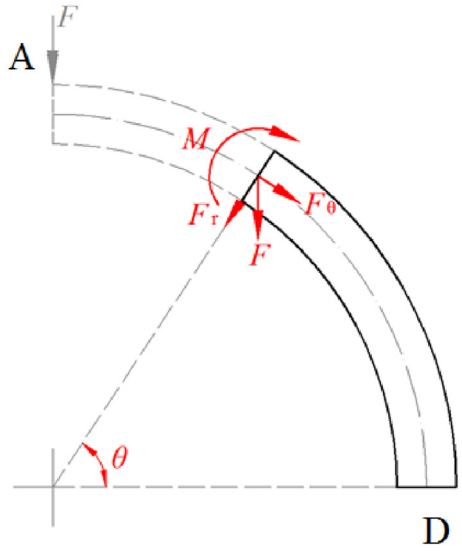

Fig. 3. Schematic diagram of a ring compressed in the radial direction.

and the total strain energy of the one quarter model is given as

$$U_{\mathrm{eq}} = \int \frac{F_\theta^2 R(1-v^2)}{2AE}\mathrm{d}\theta + \int \frac{CF_r^2 R}{2AG}\mathrm{d}\theta + \int \frac{M^2 R(1-v^2)}{2EI}\mathrm{d}\theta \tag{4}$$

where v is Poisson's ratio, G is material shear modulus, A is the cross-sectional area of the ring, R is the mean radius of the ring and can be expressed as $R = R_{\mathrm{i}} + t_{\mathrm{eq}}/2$, which is the sum of the internal radius R_{i} and half of the equivalent ring thickness t_{eq}.The parameter C in Eq. (4) is the correction factor for a rectangular cross-section in shear that takes form (Langhaar, 1962)

$$C = \frac{A}{I^2}\int_A \frac{S^2}{b^2}\mathrm{d}A \tag{5}$$

where S is the first moment of area of the infinitesimal area element about neutral axial, b is the width of the cross-section. The component forces and bending moment can be expressed as

$$F_\theta = \frac{P}{2}\cos\theta \tag{6}$$

$$F_r = \frac{P}{2}\sin\theta \tag{7}$$

$$M = M_0 + \frac{PR}{2}(1-\cos\theta) \tag{8}$$

where

$$M_0 = \frac{PR}{2}\left(\frac{2}{\pi} - 1\right) \tag{9}$$

which is the bending moment on cross section D in Fig. 3 and can be obtained by Castigliano's theorem (Timoshenko, 1930).Substituting Eqs. (6)–(8) into Eq. (4) gives

$$U_{\mathrm{eq}} = \frac{P^2(1-v^2)(R_i + t_{\mathrm{eq}}/2)}{32}\left[\frac{\pi}{AE} + \frac{C\pi}{AG} + \frac{(R_i + t_{\mathrm{eq}})^2(\pi^2-8)}{EI\pi}\right] \tag{10}$$

and thus the strain energy of that one quarter ring can be calculated.

For a flexible riser that applied to deep water environment, it is more likely to be collapsed in the plastic range (Kyriakides and Corona, 2007). Therefore, the critical pressure of the carcass is influenced by both bending stiffness and membrane stiffness since the combined effect of bending and membrane stresses plasticized the structure at its most deformed locations. In order to capture the collapse behaviour of the carcass with the equivalent layer, two kinds of equivalence should be constructed between those two structures, which are given as

$$\begin{cases} (EI)_{\mathrm{carcass}} = (EI)_{\mathrm{eq}} & \text{(11a)} \\ (EA)_{\mathrm{carcass}} = (EA)_{\mathrm{eq}} & \text{(11b)} \end{cases} \tag{11}$$

Since the bending stiffness equivalence is replaced by strain energy equivalence, then the equation set Eq. (11) can be expressed as

$$\begin{cases} U_{\mathrm{carcass}} = U_{\mathrm{eq}} = \dfrac{P^2(1-v^2)\left(R_i + \frac{t_{\mathrm{eq}}}{2}\right)}{32}\left[\dfrac{\pi}{AE_{eq}} + \dfrac{C\pi}{AG} + \dfrac{\left(R_i + \frac{t_{\mathrm{eq}}}{2}\right)^2(\pi^2-8)}{EI\pi}\right] & \text{(12a)} \\ (EA)_{\mathrm{carcass}} = (EA)_{\mathrm{eq}} & \text{(12b)} \end{cases}$$

However, solving the above equation set is a hard task since it is not possible to find an equivalent thickness to satisfy both of the two equations, i.e. Eq. (12a) and Eq. (12b). Considering that, the material Young's Modulus of the equivalent ring is chosen as an additional unknown parameter. Similar concepts are presented in the work of Clinedinst (1939); Cruz and Dias (1997). Therefore, two unknown parameters, the equivalent thickness t_{eq} and equivalent Young's Modulus E_{eq} of the equivalent ring, are going to be determined through the equation set Eq. (12), which could be expressed as

$$\begin{cases} U_{\mathrm{carcass}} = U_{\mathrm{eq}} = \dfrac{P^2(1-v^2)\left(R_i + \frac{t_{\mathrm{eq}}}{2}\right)}{32}\left[\dfrac{\pi}{AE_{eq}} + \dfrac{C\pi}{AG} + \dfrac{\left(R_i + \frac{t_{\mathrm{eq}}}{2}\right)^2(\pi^2-8)}{EI\pi}\right] \\ E\frac{A_{\mathrm{carcass}}}{L_{\mathrm{P}}} = EA_{\mathrm{eq}}t_{\mathrm{eq}} \end{cases} \tag{13}$$

Noting that the material constitutive relationship is changed when the equivalent Young's Modulus is adopted as the material of the equivalent layer. This may have an impact on the strain energy equivalence between two structures when plastic collapse failure occurs. Since the critical pressure of the plastic collapse is a yielding-based collapse pressure that is given as Eq. (14) (Timoshenko and Gere, 1963), the material yield stress $\sigma_{\mathrm{y,eq}}$ of the equivalent layer should also be regarded as a parameter awaiting solution.

$$p_{\mathrm{y}}^2 - \left[\frac{\sigma_{\mathrm{y}} t}{R} + \left(1 + 6\frac{w_0}{t}\right)p_{\mathrm{e,cr}}\right]p_{\mathrm{y}} + \frac{\sigma_{\mathrm{y}} t}{R}p_{\mathrm{e,cr}} = 0 \tag{14}$$

where p_{y} is the critical pressure of the plastic collapse of pipes, σ_{y} is the material yield stress, $w0$ is the maximum initial radial deviation from a circle, $p_{\mathrm{e,cr}}$ is the elastic critical pressure and can be calculated through Eq. (1).The basic-cell energy-equivalence concept is used to determine value of material yield stress for the equivalent ring (Nemeth, 2011; Danzi et al., 2017). Assuming that the materials for the carcass and equivalent layer are both linear and elastic, obeying Hooke's law, up to the yielding stress, then the structural strain energy density can be expressed as

$$u_\varepsilon = \frac{1}{2}\sigma_\theta\varepsilon_\theta + \frac{1}{2}\sigma_r\varepsilon_r + \frac{1}{2}\sigma_z\varepsilon_z \tag{15}$$

where σ_θ, σ_r, σ_z and ε_θ, ε_r, ε_z are the stresses and strains generated in hoop, radial and longitudinal directions separately. Thus the strain energy of the structural basic cell can be given as

$$\Psi = \int u_\varepsilon \mathrm{d}V = \int \frac{1}{2}(\sigma_\theta\varepsilon_\theta + \sigma_r\varepsilon_r + \sigma_z\varepsilon_z)\mathrm{d}V \tag{16}$$

where the V is the volume of the structure.The yielding stress of the equivalent layer can be obtained by equating the strain energy between two structures when both of them reach their material yielding stress. However, the calculation of the strain energy of the carcass is difficult as it has a complex profile. To simplify this calculation, two assumptions are made herein: a) Assume that the strains in radial and longitudinal directions are negligible; b) Assume that the variation of hoop strains across the thickness of the layer wall can be neglected. With those two assumptions, Eq. (16) can be rewritten as

$$\Psi = \int \frac{1}{2}\sigma_\theta \varepsilon_\theta dV = \int \frac{1}{2}\frac{\sigma_\theta^2}{E} dV \tag{17}$$

By equating the strain energy at the onset of material yielding between the carcass and the equivalent layer

$$\Psi_{carcass} = \Psi_{eq} \tag{18}$$

The yielding stress of the equivalent layer takes the form

$$\sigma_{eq,y} = \sqrt{\frac{E_{eq}\sigma_y^2}{E}\frac{V_c}{V_{eq}}} \tag{19}$$

where the σ_y is the yielding stress of the carcass material, V_c and V_{eq} are the volumes of the carcass and equivalent layer, separately. With the values of equivalent thickness t_{eq} and equivalent Young's modulus E_{eq} obtained from Eq. (13), the yielding stress $\sigma_{eq,y}$ of the equivalent layer can be calculated by Eq. (19). Finally, the geometric and material properties for the equivalent layer are both determined.

A brief step-by-step methodology is presented as follow to give a clear clarification of the proposed method:

Step 1, calculating the strain energy $U_{carcass}$ of the carcass with a given radial compression load P numerically (A feasible numerical simulation is presented in Section 3 to show how to provide a reliable strain energy for the proposed method).

Step 2, determining equivalent layer properties t_{eq} and E_{eq} by substituting the values of Ucarcass and P into equation set Eq. (13).

Step 3, determining the equivalent yielding stress $\sigma_{eq,y}$ with the above t_{eq} and E_{eq} by using Eq. (19).

With all the above-mentioned equivalent properties, t_{eq}, E_{eq} and $\sigma_{eq,y}$, have been solved, an equivalent layer model can be built for collapse studies.

3. Numerical simulation for strain energy calculation

As above-mentioned, the strain energy $U_{carcass}$ of the carcass was required as an input in Eq. (13) to calculate the equivalent properties for the homogeneous layer, therefore, this section is mainly focused on how to provide such a strain energy with FE simulation. In this section, a feasible FE simulation is presented to show how to calculate the strain energy of the carcass and its reliability was verified by the test data of Tang et al. (2016). This FE simulation was referred to the experimental tests conducted by Tang et al. (2016), as shown in Fig. 4. In their work, the compression tests were performed on three kinds of carcass samples with inner diameters of 6 in., 7 in. and 8 in. Fig. 5 shows a typical cross-sectional profile of the carcass and the geometric and material properties of the samples are summarized in Table 1.

3.1. Radial compressed carcass model

A 3D model of the interlocked carcass was constructed by using Abaqus 6.13 software. Two pitches of the carcass were considered as a representative length and solid elements were adopted in this 3D model, as shown in Fig. 6. The lay angle of the carcass strips was neglected since it is not responsible for the important effects in collapse prediction according to the study of Gay Neto and Martins (2012). Due to the symmetry of the carcass structure, only half of the carcass ring was modelled. A rigid plate was also modelled to support the carcass model.

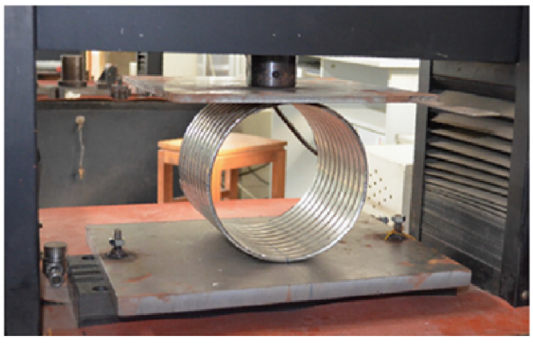

Fig.4. Experimental set-up of carcass radial compression (Tang et al., 2016)

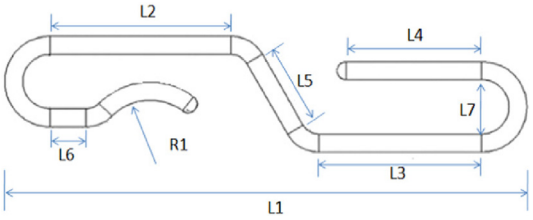

Fig. 5. Schematic diagram of the carcass profile (Tang et al., 2016).

Table 1
Geometric and material properties of the carcass samples (Tang et al., 2016).

Sample ID (in.)	6	7	8	Sample ID (in.)	6	7	8
Pitch length Lp (mm)	14.88	17.00	12.55	$L5$ (mm)	1.80	2.61	2.41
Carcass strip thickness t (mm)	0.90	0.96	1.30	$L6$ (mm)	0.00	2.02	0.00
$L1$ (mm)	26.20	31.42	23.43	$L7$ (mm)	1.77	2.67	2.12
$L2$ (mm)	10.36	10.40	7.44	$R1$ (mm)	4.18	3.75	4.18
$L3$ (mm)	8.96	10.91	7.47	E (GPa)	206	206	206
$L4$ (mm)	5.90	8.01	4.39	ν	0.3	0.3	0.3

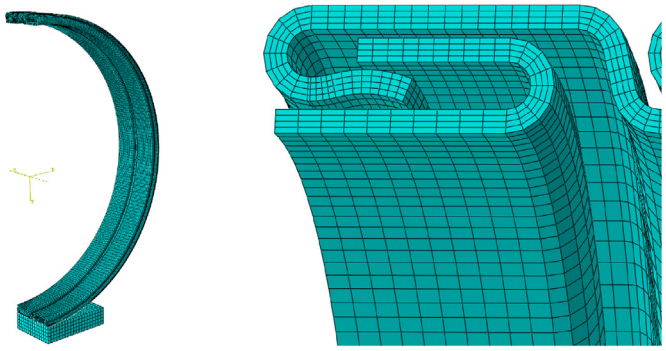

Fig. 6. Radial compressed carcass model, (a) whole view and (b) detailed view.

The boundary conditions considered in the half carcass model were imposed as: (a) symmetry condition on the carcass cross sections, (b) the displacements of the portion of the carcass contacted with the bottom rigid plate are constrained in all directions and (c) the displacements of the side cutting sections are constrained in longitudinal direction. The supported rigid plate was fully fixed. Those applied boundary conditions are shown in Fig. 7.

Displacement couplings were set on the carcass profile to simulate a carcass layer with infinite pitches. MPC constraints were imposed on the cutting regions since there were only two pitches presented in this model, as shown in Fig. 8. The loading force was applied on four top points of the carcass evenly, which is shown in Fig. 9. This loading type was chose due to two reasons: one was that the contact issue between the top loading plate and carcass could be eliminated; the other was the computational results from the FE models with and without the top loading plate were almost the same. Since the carcass was compressed within the elastic range (according to the test data of Tang et al. (2016)), the stress concentration at those four points had little impact on the calculation results.

Since the self-contact might lead to possible stiffness reduction of the carcass, the Penalty Method was chosen to deal with that contact problem. A surface-to-surface formulation was used for the contact

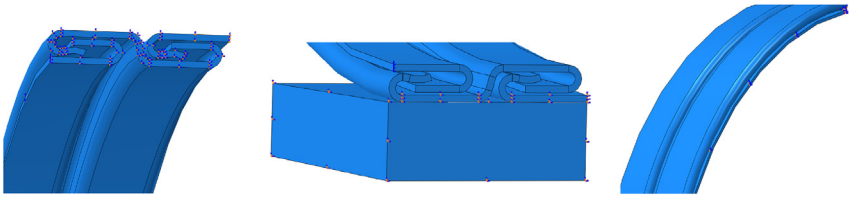

Fig. 7. Boundary conditions applied onto the model (a) symmetry condition, (b) displacement constraints of the portion contacted with the rigid plate (c) displacement constraints of the side cutting section.

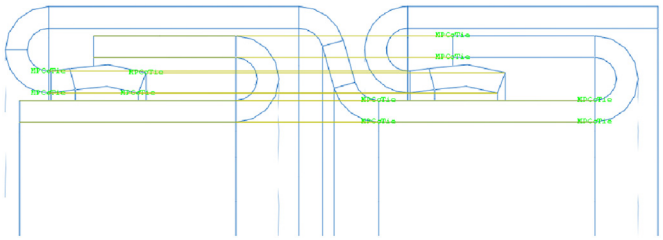

Fig.8. Coupling details considered in the compressed carcass model

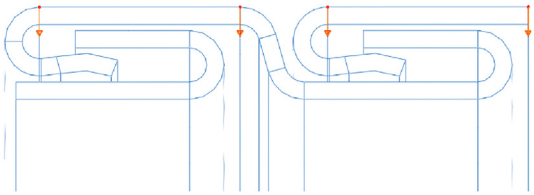

Fig. 9. Compression force applied to the carcass model.

between the carcass strips and the normal penalty stiffness factor was defined as 0.1. Friction was also considered in the models to account for the related energy dissipation. The friction factor was defined as 0.13 at the self-contact regions. The values of those factors were referred to Tang et al. (2016).

3.2. Model validation

The curves of radial deformation versus compression load of each carcass samples were recorded by Tang et al. (2016), which are shown as Fig. 10. The maximum loading displacement was controlled to make sure that the maximum ovalization of all the samples lower than 3%. It can be seen from Fig. 10 that the radial compression stiffness of the carcass samples become stable after the compression loads reach certain

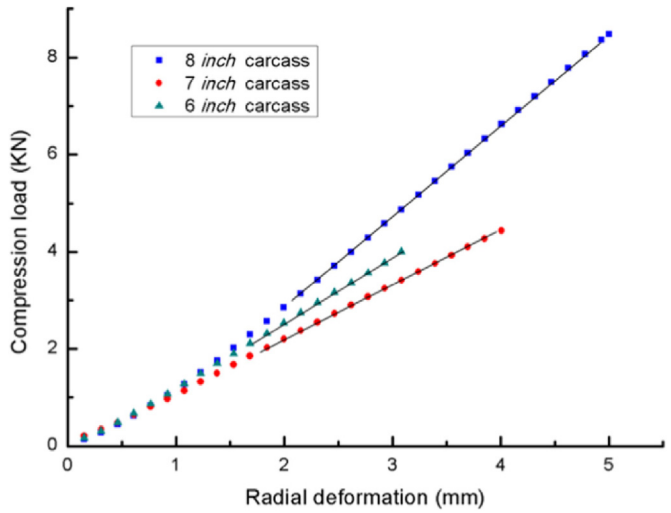

Fig. 10. Test results of the radial compression of the carcass test pieces (Tang et al., 2016).

Table 2
Load-displacement results comparison for each case.

Sample ID	Compression loads (kN)		2	3	4	6
6″	Radial displacements (mm)	Experimental	1.60	2.35	–	–
		numerical	1.43	2.16	–	–
7″		Experimental	1.90	2.80	–	–
		Numerical	2.07	3.10	–	–
8″		Experimental	–	–	2.60	3.70
		Numerical	–	–	2.66	3.99

values. This represents that the gaps within the carcass samples were diminished with the increased compression loads and finally the samples were compressed into compact structures. In order to reflect the structural stiffness of a compact carcass, the compression loads applied to the numerical models were 2 kN and 3 kN for the 6 in. and 7 in. carcass and 4 kN and 6 kN for the 8 in. carcass. The mean value of the displacements at the loading nodes were obtained and compared to the test results.

The comparison results are listed in Table 2 and it can be seen that the radial displacements provided by numerical models agree well with the test results for each loading case. The maximum error that given by the numerical models is just around 10%, showing that those numerical models can be a reliable approach to extract the strain energy of the carcass.

4. Verification of the proposed equivalent method

With the methodology presented in the previous two sections, an equivalent layer model of the carcass can be constructed. In this section, the prediction accuracy of that equivalent layer model was verified by a full 3D carcass model presented in the work of Gay Neto and Martins (2012). This model has been widely used by many researchers and was recreated to provide a critical pressure for comparison purpose. In the meanwhile, some other equivalent layer models based on the existing equivalent methods were also built in order to give a comprehensive comparison.

4.1. Full 3D model for the comparison purpose

To examine the effectiveness of the proposed equivalent method in predicting the critical pressure of the carcass, an example presented by Gay Neto and Martins (2012) was adopted. In that example, two layers, the carcass and the polymeric inner liner were considered. This inner liner only acted as a load transmitter during the loading process. The carcass profile is sketched in Fig. 11 and its geometrical and material

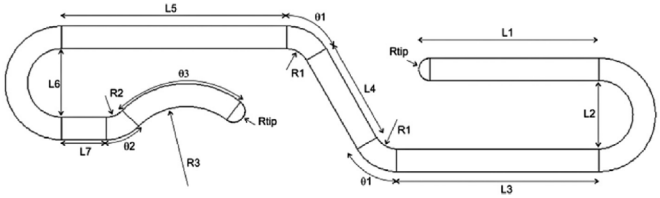

Fig. 11. Schematic diagram of the carcass profile (Gay Neto and Martins, 2012).

Table 3
Geometrical and material properties of Gay Neto's carcass model (Gay Neto and Martins, 2012).

Internal diameter (in.)	4	θ_1 (deg)	60
Pitch length L_p (mm)	16	θ_2 (deg)	45
Carcass strip thickness t (mm)	1.00	θ_3 (deg)	90
L_1 (mm)	8.00	R_1 (mm)	1.00
L_2 (mm)	3.00	R_2 (mm)	1.00
L_3 (mm)	9.00	R_3 (mm)	3.00
L_4 (mm)	4.50	E (GPa)	200
L_5 (mm)	10.00	ν	0.3
L_6 (mm)	3.00	Yielding stress σ_y (MPa)	600
L_7 (mm)	2.00	Tangent modulus E_t	2000
R_{tip} (mm)	0.50	(after yielding stress) (MPa)	

are given in Table 3.

A bi-linear constitutive model was adopted to describe the elasto-plastic property of the carcass material. The carcass material behaves linearly and elastically before reaching its yielding stress. Once the yield stress is reached, another linear behaviour is assumed with a slope given by the material tangent modulus. For the inner liner, a multi-linear elastic material constitutive model was used to describe its material property. The material stress-strain curves for both carcass and inner liner are plotted in Fig. 12 and Fig. 13 separately.

Considering that the collapse of the carcass was an axisymmetric issue, only half of the carcass was modelled so that making the solution computational faster. Two displacement conditions were imposed as the model boundary conditions: a) symmetry condition in plane xy and b) a fully fixed external edge of the inner liner (the red line displayed in Fig. 14b). Fig. 14 shows the whole model and its applied boundary condition. The pressure applied onto the external surface of the inner liner was the only load considered in the models. To capture the critical pressure of the carcass subjected to the external pressure, the Riks solution algorithm was used in the numerical models. This captured critical pressure was regarded as a reference value that judging the predictive accuracy of the equivalent layer models.

4.2. Equivalent layer models

With the equivalent properties determined by the proposed method, a finite element model of the equivalent layer (Model A) was constructed. That equivalent layer FE model is shown in Fig. 15. The external pressure was applied onto the external surface of the inner liner to compress the whole model till the collapse occurs. The critical collapse pressure of the equivalent model was read through its result files and then compared with that of the full 3D model.

To give a more comprehensive comparison, some other equivalent models based on the existing equivalent methods were also constructed.

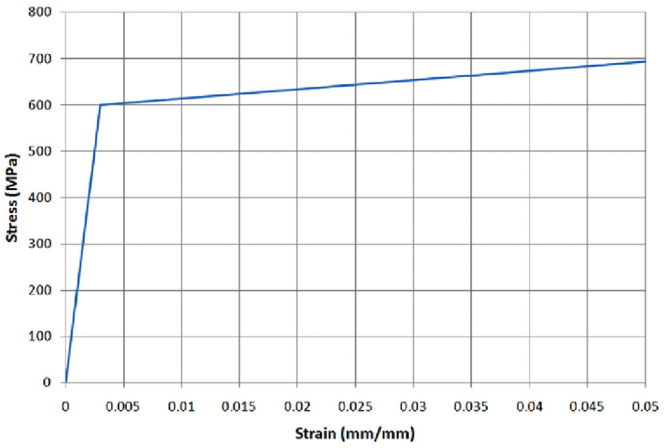

Fig.12. Stress-strain curve of the carcass material (Gay Neto and Martins, 2012)

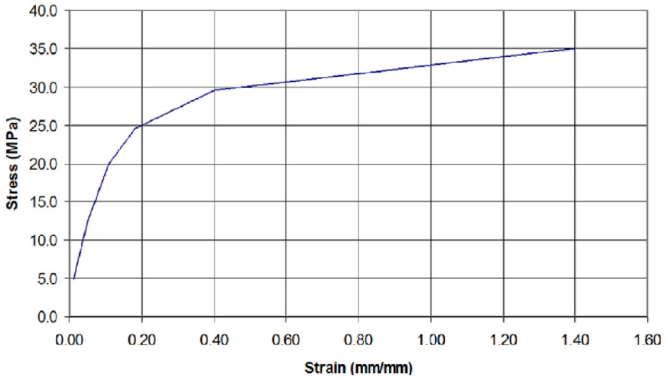

Fig. 13. Stress-strain curve of the inner liner material (Gay Neto and Martins, 2012).

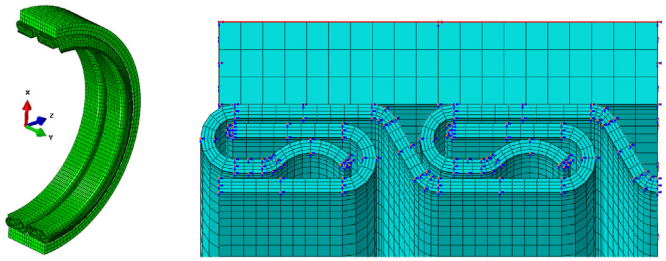

Fig. 14. A) numerical model for critical pressure prediction and b) the imposed boundary conditions.

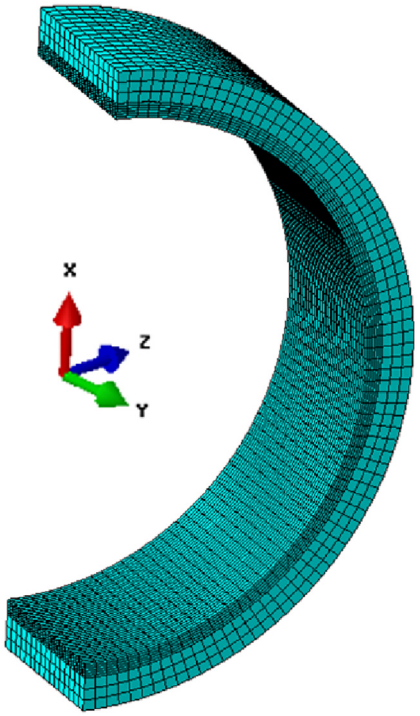

Fig. 15. Whole view of the equivalent layer model.

Those methods are proposed based on different structural property equivalences are presented as follows: a) Area equivalence (Model B) This method obtains the thickness of the equivalent layer by equating the cross-sectional area between the carcass and the equivalent layer, which can be expressed as (Zhang et al., 2003)

$$t_{eq,1} = \frac{A}{L_p} \tag{20}$$

b) Bending stiffness equivalence per area (Model C) This method was employed by De Sousa et al. (2001) that obtaining the thickness by equating sectional bending stiffness between two structures. The equation takes the form

$$t_{eq,2} = \sqrt{\frac{12I_{Gmin}}{A}} \tag{21}$$

where I_{Gmin} is the minimum moment of inertia of the carcass cross section. c) Bending stiffness equivalence per length (Model D) This method is similar to the second one but build the bending stiffness equivalence based on unit length (Martins et al., 2003). Therefore, the equivalent thickness can be calculated as

$$t_{eq,3} = \sqrt[3]{\frac{12(1+\psi)I_{Gmin}}{L}} \tag{22}$$

where L is the axial length of the carcass and ψ is the rate of superposition of the carcass profiles. The value of the ψ depends on the profile geometry and the pitch considered, which could be calculated by using the superposed length L_{super} between two profiles in a pitch (Gay Neto and Martins, 2012)

$$\psi = \frac{L_{super}}{L_p} \tag{23}$$

d) Circumferential strain energy equivalence (Model E) This method is proposed by Tang et al. (2016) which build a strain energy equivalence between two structures that with a specific structural strain condition: uniform hoop strain is the only strain type that allowed to be generated. The calculation of the strain energy $\Psi_{carcass}$ of the carcass is completed through numerical models and a displacement load u_θ that is linearly proportional to the radial length is applied onto the carcass profile to help create uniform hoop strain ε_θ, which is given as

$$u_\theta = \frac{\pi}{2} r_x \varepsilon_\theta \tag{24}$$

where r_x is the radial length of the carcass. The strain energy of the equiva-lent layer that with the same uniform hoop strain ε_θ is given as

$$\Psi_{eq} = \int \frac{1}{2}\sigma_\theta \varepsilon_\theta dV = \frac{\pi}{4} A_1 \varepsilon_\theta^2 RLt_{eq} \tag{25}$$

The parameter $A1$ within Eq. (25) takes the form

$$A_1 = E\frac{1-v}{(1+v)(1-2v)} \tag{26}$$

and thus the equivalent thickness is given as

$$t_{eq,4} = \frac{\Psi_{carcass}}{\frac{\pi}{4} A_1 \varepsilon_\theta^2 RL} \tag{27}$$

The geometric and material properties of those the equivalent layer models are presented in Table 4. The internal diameter and longitudinal length of all the equivalent layer models were identical with the 4 in. carcass full model.

Table 4
Geometrical and material properties of the equivalent layer.

Model	Thickness (mm)	Young's modulus (GPa)	Yielding stress (MPa)
Model A	2.85	244.9	691
Model B	3.49	200	600
Model C	6.32	200	600
Model D	5.18	200	600
Model E	2.59	200	600

Fig. 16. Reference line for measuring the radial displacement of FE models.

4.3. Comparison of the critical pressure predictions

The Arc length technique was employed to capture the snap-through occurrence of each finite element model. It was necessary to choose a representative radial displacement value for each cross section in the numerical models since each point had a different displacement value. A reference line was chosen from the internal surface of numerical models (full 3D model as well as equivalent models) that identified in Fig. 16. The mean value of the radial displacement of the nodes on that reference line was regarded as the radial displacements of the models subjected to external pressure.

The critical pressure and the radial displacement at the critical pressure provided by each model are summarized in Table 5. The curves of radial displacement versus external pressure are plotted in Fig. 17.

According to the black solid line plotted in Fig. 17, a stiffness reduction of the full carcass model appeared when the external pressure reaches 12 MPa approximately. It represents the occurrence of the material plasticity, which was further developed with the increasing external loads. Model B gave a linear behaviour that agreed well with the full model before the occurrence of plastic stresses. However, it failed to capture the following collapse behaviour of the full carcass model because the area equivalence considered in this model cannot build a relationship to its material properties. The results came from Model C and D deviated considerably from that of the full model. The methods used in those two models calculated the inertial moment based on the geometric cross section of the carcass purely, which neglected the contact and fiction-induced stiffness reduction. That could explain that why both of the two models have much higher layer thicknesses and overestimate the critical pressure of the carcass. By contrast, the critical pressure provided by Model A and Model E were relatively conservative. As stated above, the thickness of Model E was determined based on structural strain energy that generated by uniform hoop strain of the carcass. In other word, this model was constructed based on membrane stiffness equivalence only and therefore underestimates the overall structural stiffness of the carcass. As a result, it gave an over-conservative prediction on the critical pressure of the carcass. Among those equivalent models, Model A provided a much closer prediction to the critical pressure of the carcass according to Fig. 17. The predictive error on critical pressure between the Full model and Model A was just around 6.5%, which showed that model built with both geometric and material equivalences can provide a better prediction of the critical pressure of the carcass.

5. Conclusion and discussion

Predicting the critical collapse of flexible risers accurately is a difficult task and efficient calculation methods are always demanded. Dealing the complex carcass structure with an equivalent layer is the first and foremost step in collapse analyses of the flexible risers. Up till now, various equivalent methods are developed for constructing such an equivalent layer. However, most of them are proposed by imposing equity between the carcass and homogeneous layer for one certain property and the layer thickness has always been the only output for the equivalent layer. As a result, their predictions of the critical pressure of the carcass often result in considerable errors.

Considering that, an equivalent layer method is proposed in this paper by considering the strain energy and membrane stiffness

Table 5
Critical pressure and radial displacement comparison between full and equivalent models.

Model	Critical pressure (MPa)	Radial displacement (mm)	Error in critical pressure prediction (%)
Full 3D model	18.73	1.57	–
Model A (the proposed method)	17.52	1.41	−6.46
Model B (area equivalence)	20.37	1.30	8.76
Model C (bending stiffness equivalence per area)	47.87	0.75	155.58
Model D (bending stiffness equivalence per length)	35.46	0.96	89.32
Model E (circumferential strain energy equivalence)	14.39	1.43	−23.17

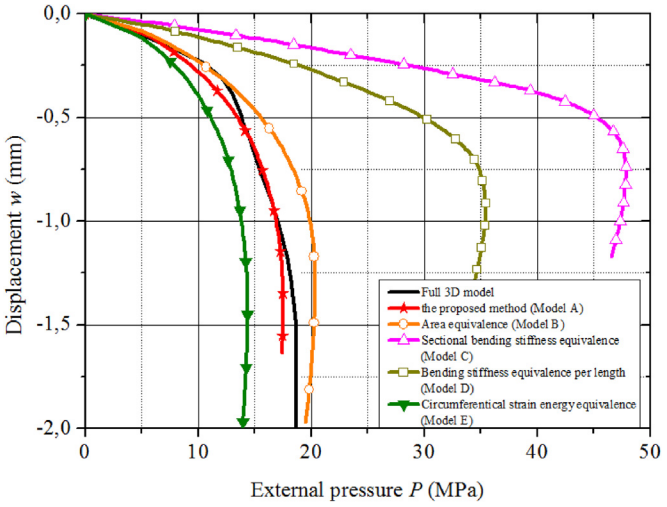

Fig. 17. Comparison of the curves of external pressure versus radial displacement.

simultaneously. Essentially speaking, this method is proposed based on membrane and bending stiffness equivalence between the carcass and equivalent layer structures. However, due to the fact that there is no available approach to calculate the actual bending stiffness of the carcass, the strain energy was adopted as an alternative. The strain energy of the carcass was first obtained through 3D FE carcass models and then used to determine the equivalent properties, the layer thickness and Young's modulus, for the equivalent layer in combination with membrane stiffness equivalence. Using such a 3D FE carcass model is due to the fact that there is no available mathematical model yet for the strain energy calculation of such interlocked layer structures. Although this is a limitation of the proposed equivalent layer method, it offers an approach to consider the self-contact issue of the carcass. Additionally, a material equivalent yield stress was also determined based on that obtained equivalent Young's modulus to account for the plastic collapse of deep-water flexible risers.

A set of models were built to examine the reliability of the proposed method as well as other existing methods. From the comparison results, the model constructed based on the proposed method gave the closest prediction on the critical collapse pressure of the carcass, only with an error of 6.5%. It indicates that this strain energy based equivalent layer method is able to consider the actual structural stiffness of the carcass and can be a reliable and effective tool for the collapse study of flexible risers.

Acknowledgments

This work was supported by the China Scholarship Council [grant number 201606950011].

References

Clinedinst, W.O., 1939. A rational expression for the critical collapsing pressure of pipe under external pressure. Am. Pet. Institute, Drill. Prod. Pract 383–391.
Cooke, N., Kenny, S., 2014. Comparative study on the collapse response of flexible pipe using finite element methods. In: Proceedings of the International Conference on Offshore Mechanics and Arctic Engineering, OMAE2014–23306, (San Francisco, California, USA).
Cruz, F.T.L., Dias, C.A.N., 1997. Structural analysis of flexible pipe using finite element method. In: Proceedings of the 7th International Offshore and Polar Engineering Conference, Honolulu, USA.
Cuamatzi-Melendez, R., et al., 2017. Finite element and theoretical analyses of bisymmetric collapses in flexible risers for deepwaters developments. Ocean Eng. 140, 195–208.
Danzi, F., et al., 2017. Equivalent plate model of curvilinear stiffened panels. In: Proceedings of the 7th International Conference on Mechanics and Material in Design, Albufeira, Portugal.
De Sousa, J.R.M., et al., 2001. Local mechanical behavior of flexible pipes subjected to installation loads. In: Proceedings of the International Conference on Offshore Mechanics and Arctic Engineering, OMAE2001/PIPE-4102, Rio de Janeiro, Brazil.
Edmans, B., 2014. Finite element studies for assessment of collapse modelling methodologies for unbonded flexible pipes. In: Proceedings of the Offshore Technology Conference, OTC 24815, (Kuala Lumpur, Malaysia).
Fergestad, D., et al., 2017. Handbook on Design and Operation of Flexible Pipes. Technical Report. MARINTEK.
Gay Neto, A., Martins, C.A., 2012. A comparative wet collapse buckling study for the carcass layer of flexible pipes. J. Offshore Mech. Arctic Eng. 134, 1–9.
Gay Neto, A., et al., 2009. A numerical simulation of crushing in flexible pipes. In: 20th International Congress of Mechanical Engineering, COBEM 2009, Gramado, RS, Brazil.
Kyriakides, S., Corona, E., 2007. Mechanics of Offshore Pipelines. Volume 1: Buckling and Collapse. Elsevier, Oxford, UK.
Langhaar, H.L., 1962. Energy Methods in Applied Mechanics. Wiley, New York, USA.
Loureiro, W.C., Pasqualino, I.P., 2012. Numerical-analytical prediction of the collapse of flexible pipes under bending and external pressure. In: Proceedings of the International Conference on Offshore Mechanics and Arctic Engineering, OMAE2012-83476, Rio de Janeiro, Brazil.
Luppi, A., Cousin, G., O sullivan, R., 2014. Deep water hybrid riser systems. In: Proceedings of the Offshore Technology Conference, OTC 24802, (Kuala Lumpur, Malaysia).
Martins, C.A., et al., 2003. Structural behavior of flexible pipe carcass during launching. In: Proceedings of the International Conference on Offshore Mechanics and Arctic Engineering, OMAE2003-37053, (Cancun, Mexico).
National Oilwell Varco, 2014. Floating Production Systems: Dynamic Flexible Risers.
Nemeth, M., 2011. A Treatise on Equivalent-plate Stiffnesses for Stiffened Laminated-composite Plates and Plate-like Lattices. NASA TP-2011–216882.
NOV, Flexibles, 2015. We Power the Industry that powers the World. National Oilwell Varco.
Suleiman, M.T., 2002. The Structural Performance of Flexible Pipes. DSc. Thesis. Iowa State University, Iowa, USA.
Tang, M., et al., 2016. Buckling collapse study for the carcass layer of flexible pipes using a strain energy equivalence method. Ocean Eng. 111, 209–217.
Technip, 2014. Flexible Pipe: How Technip Offers a Broad Range of Flexible Pipe Systems with the Most Advanced Integrated Solutions for Deepwater and Ultra Deepwater Field Developments. Technip Company.
Timoshenko, S.P., 1930. Strength of Materials. Part 1: Elementary Theory and Problems. McGraw-Hill, New York, USA.
Timoshenko, S.P., Gere, J., 1963. Theory of Elastic Stability. McGraw-Hill, New York, USA.
Vidigal da Silva, J., Damiens, A., 2016. 3000 m water depth flexible pipe configuration portfolio. In: Proceedings of the Offshore Technology Conference, OTC 26933, (Houston, Texas, USA).
Wolodko, J., DeGeer, D., 2006. Critical local buckling conditions for deepwater pipelines. In: Proceedings of the International Conference on Offshore Mechanics and Arctic Engineering, OMAE2006–92173, (Hamburg, Germany).
Zhang, Y., et al., 2003. State of the art analytical tools improve optimization of unbonded flexible pipes for deepwater environments. In: Proceedings of the Offshore Technology Conference, OTC 15169, (Houston, Texas, USA).